

Structural topology optimization on dynamic compliance at resonance frequency in thermal environments

Xiongwei Yang · Yueming Li

Received: 8 January 2013 / Revised: 1 June 2013 / Accepted: 8 June 2013 / Published online: 27 July 2013
© Springer-Verlag Berlin Heidelberg 2013

Abstract This paper carries out topology optimization to minimize structural dynamic compliance at resonance frequencies in thermal environments. The resonance response is the main dynamic component, minimization of which could possibly change structural dynamic characteristics significantly. A bi-material square plate subjected to uniform temperature rise and driven by harmonic load is investigated in pre-buckling state. The compressive stress induced by thermal environment is considered as pre-stress in dynamic analysis, which could reduce stiffness of the structure and alter the optimal topology. Sensitivity analysis is carried out through adjoint method efficiently. As natural frequencies are constantly changing during the optimization, the associated sensitivity should be calculated in which multiple-frequency case is briefly discussed. Mode switching may occur during the optimization, and mode tracking technique is adopted. Numerical results show that the topology is mainly determined by the excited modes, and could be altered by the location of the applied load if different modes are excited. The natural frequencies become larger in optimal design and the dynamic compliance decreases in nearby frequency band. The critical buckling temperature increases as optimization

proceeds, indicating the structure is always in pre-buckling state.

Keywords Topology optimization · Dynamic compliance · Resonance response · Thermal environment

1 Introduction

The thermal-acoustic environment is quite critical during the flight envelop of hypersonic vehicles, posing major challenges in structural design. One is to provide light-weight structures with ideal dynamic characteristic in thermal conditions. The thermal environment could induce compressive stresses that may alter structural dynamic characteristic and even cause buckling. Resonance response under acoustic excitation is main dynamic component, optimization aimed at which could probably find such optimal designs.

Since the landmark work of Bendsøe and Kikuchi (1988), topology optimization has been extended to various kinds of fields. The precursory work in dynamic area was carried out by Diaz and Kikuchi (1992), in which the shape and topology optimization of structure to maximize a natural frequency was studied using homogenization method. The homogenization method was then extended to a frequency response optimization problem for both optimal layout and reinforcement of an elastic structure (Ma et al. 1993) and more general eigenvalue and vibrating problems (Ma et al. 1995). Yang et al. (1999) presented evolutionary method for structural topology optimization subjected to frequency constraints, in which the sensitivity of multiple frequencies was simplified by taking an average. Min et al. (1999) applied the homogenization method to tran-

National Natural Science Foundation of China (91016008, 91216107, 11021202).

X. Yang · Y. Li (✉)
State Key Laboratory for Strength and Vibration of Mechanical Structures, School of Aerospace, Xi'an Jiaotong University, Xi'an Shaanxi, 710049, People's Republic of China
e-mail: liyueming@mail.xjtu.edu.cn

sient problems of vibrating structures, to find the best that minimizes the dynamic compliance within a specified time interval. Jog (2002) studied the topology configuration of structures subjected to periodic loadings from the global and local dynamic constraints, i.e. overall dynamic compliance and response at a specific point respectively. Du and Olhoff (2007) employed SIMP (Solid Isotropic Material with Penalization) interpolation model to maximize the natural frequency of higher order, or the gap between two consecutive natural frequencies of given orders; both simple and multiple natural frequencies were considered.

It is known that thermal stress may change the stiffness of structures, and alter the dynamic characteristic (Cook et al. 1989). Pedersen (2001, 2002) optimized the static compliance or eigenvalues of pre-stressed isotropic and laminated plates in MEMS design, the stresses were given at different constant levels which are in fact changing during the optimization. Chen et al. (2003) investigated the design optimization for structural thermal buckling, considering heat conduction at the same time. Both direct and adjoint methods were discussed, and the former was employed due to complexity of the adjoint method. Yang and Li (2013) carried out topology optimization to minimize the structural dynamic compliance in thermal environments using adjoint sensitivity analysis, fully considering the changing thermal stress and its relationship with design variables.

Optimization involving resonance (or natural) frequencies mainly focuses on minimization or maximization of given order eigenvalues, such as Yang et al. (1999), Du and Olhoff (2007). Literature survey shows that few works have been conducted in frequency response problems. Belegundu et al. (1994) described a general way to minimize sound radiation of a baffled plate, in which the radiated sound power within a band was approximated by the sum of the power at each resonance frequency.

This study could be regarded as an extended work of Yang and Li (2013), aimed at the structural dynamic compliance at resonance frequencies in thermal environments. It is assumed that resonance frequency equals natural frequency and the differences between them are neglected. A bi-material square plate subjected to uniform temperature rise and driven by harmonic load is investigated. The thermal stress is considered as pre-stress in dynamic analysis, and sensitivity analysis is carried out efficiently with adjoint method. The main difference from previous work in Yang and Li (2013) is that the resonance frequencies are constantly changing during the optimization; thus the associated sensitivity needs to be calculated. It should be noticed that mode switching may occur, and mode tracking technique is adopted to ensure a smooth convergence. Special

case involving multiple natural frequencies is also briefly addressed.

2 Dynamic structure in thermal environments

One of the common ways to analyze dynamic problems in thermal environments is to treat the thermal stress as pre-stress, leading to a linear stress-stiffening dynamic formula (Cook et al. 1989)

$$(\mathbf{K} + \mathbf{K}_G - \omega^2 \mathbf{M}) \Phi = \mathbf{0} \quad (1)$$

$$(\mathbf{K} + \mathbf{K}_G - \omega^2 \mathbf{M}) \mathbf{U} = \mathbf{F} \quad (2)$$

where \mathbf{K} , \mathbf{M} are stiffness and mass matrices respectively; Φ is mass-normalized mode vector; \mathbf{U} is dynamic displacement response vector; \mathbf{F} is amplitude vector of the external load; $\omega = 2\pi f$ is natural circle frequency. \mathbf{K}_G refers to geometric stiffness for bending induced by the in-plane thermal stresses

$$\mathbf{K}_G = \sum_i \int_{A_i} \mathbf{G}^T \langle \sigma \rangle \mathbf{G} dA \quad (3)$$

where σ is membrane stress vector; $\langle \rangle$ means to write vector into Voigt matrix; \mathbf{G} is a nonlinear strain-displacement matrix; A_i is area of element i .

Please note that damping should be considered to get resonance response. However, it is neglected in the formulas just for simplicity.

For a plate subjected to temperature rise from the ambient, the in-plane stress can be described with the plane-stress constitutive equation if the temperature change across the thickness is uniform,

$$\sigma = \mathbf{D}_m(\epsilon - \alpha \Delta \mathbf{T}) = E \mathbf{D} \epsilon - \beta \mathbf{D} \Delta \mathbf{T} \quad (4)$$

where E , α , $\beta = E\alpha$ are elastic modulus, thermal expansion coefficient and thermal stress coefficient respectively; \mathbf{D}_m is membrane elasticity matrix; $\Delta \mathbf{T}$ is the temperature rise vector. The strain ϵ can be obtained through the solution of a static thermal displacement equation

$$\mathbf{K} \mathbf{U}_t = \mathbf{F}_t \quad (5)$$

where \mathbf{U}_t is thermal displacement vector; \mathbf{F}_t refers to equivalent thermal force induced by the uniform temperature rise.

The thermal stress coefficient β introduced here is to avoid incompatibility that may occur between the stiffness and the thermal load in material interpolation model (Gao and Zhang 2010; Yang and Li 2013).

3 Optimization problem

The topology optimization problem for minimizing the dynamic compliance of the bi-material plate in the thermal environment can be stated as

$$\begin{aligned}
 \min \quad & C = \{\mathbf{F}^T \mathbf{U}\}^2 \\
 \text{s.t.} \quad & (\mathbf{K} + \mathbf{K}_G - \omega^2 \mathbf{M}) \mathbf{U} = \mathbf{F} \\
 & (\mathbf{K} + \mathbf{K}_G - \omega^2 \mathbf{M}) \boldsymbol{\Phi} = \mathbf{0} \\
 & \mathbf{K} \mathbf{U}_t = \mathbf{F}_t \\
 & \sum_i V_i \zeta_i \leq V \\
 & \zeta_i \in (0, 1)
 \end{aligned} \tag{6}$$

where ζ_i is the design variable, denoting the artificial volume fraction of material 1 (the stiffer of the two materials) in the element i ; V_i is volume of the element i ; V is the maximum volume of material 1.

The difference from the optimization equation in Yang and Li (2013) is that ω refers to the resonance circle frequency and that the mode analysis equation is included here. At each iteration, the 3rd constraint equation is first solved to calculate the displacement \mathbf{U}_t . The geometric stiffness matrix \mathbf{K}_G can then be obtained through (3) and (4). And the first two constraint equations can be solved.

4 Sensitivity analysis

The sensitivity of the objective function C can be written as (Bendsøe and Sigmund 2003)

$$\frac{dC}{d\zeta_i} = \boldsymbol{\Psi}^T \left(\frac{d\mathbf{K}}{d\zeta_i} + \frac{d\mathbf{K}_G}{d\zeta_i} - \omega^2 \frac{d\mathbf{M}}{d\zeta_i} - \mathbf{M} \frac{d\omega^2}{d\zeta_i} \right) \mathbf{U} \tag{7}$$

where $\boldsymbol{\Psi}$ is solution to the adjoint problem

$$(\mathbf{K} + \mathbf{K}_G - \omega^2 \mathbf{M}) \boldsymbol{\Psi} = -2 \{\mathbf{F}^T \mathbf{U}\} \mathbf{F} \tag{8}$$

The sensitivity of natural circle frequency ω is inclusive in (7) as this is a dynamic optimization on resonance response,

$$\frac{d\omega^2}{d\zeta_i} = \boldsymbol{\Phi}^T \left(\frac{d\mathbf{K}}{d\zeta_i} + \frac{d\mathbf{K}_G}{d\zeta_i} - \omega^2 \frac{d\mathbf{M}}{d\zeta_i} \right) \boldsymbol{\Phi} \tag{9}$$

If ζ_i changes, only \mathbf{K} and \mathbf{M} at the element i will vary as the design variable denotes the artificial fraction of the stiffer material at each element, while \mathbf{K}_G at all elements will vary since the whole thermal displacement field of the structure

has been altered. Therefore, (7) and (9) can be written at element level,

$$\begin{aligned}
 \frac{dC}{d\zeta_i} &= \boldsymbol{\Psi}_i^T \left(\frac{d\mathbf{K}_i}{d\zeta_i} - \omega^2 \frac{d\mathbf{M}_i}{d\zeta_i} - \frac{d\omega^2}{d\zeta_i} \mathbf{M}_i \right) \mathbf{U}_i \\
 &+ \sum_j \boldsymbol{\Psi}_j^T \frac{d\mathbf{K}_{Gj}}{d\zeta_i} \mathbf{U}_j
 \end{aligned} \tag{10}$$

$$\begin{aligned}
 \frac{d\omega^2}{d\zeta_i} &= \boldsymbol{\Phi}_i^T \left(\frac{d\mathbf{K}_i}{d\zeta_i} - \omega^2 \frac{d\mathbf{M}_i}{d\zeta_i} \right) \boldsymbol{\Phi}_i \\
 &+ \sum_j \boldsymbol{\Phi}_j^T \frac{d\mathbf{K}_{Gj}}{d\zeta_i} \boldsymbol{\Phi}_j
 \end{aligned} \tag{11}$$

The derivatives of \mathbf{K} , \mathbf{M} in (10) and (11) can be obtained based on RAMP (Rational Approximation of Material Properties) interpolation model (Stolpe and Svanberg 2001).

The derivative of \mathbf{K}_G can be derived from (3) and (4) (Yang and Li 2013), and for the element j one has

$$\begin{aligned}
 \frac{d\mathbf{K}_{Gj}}{d\zeta_i} &= \frac{dE_j}{d\zeta_i} \int_{A_j} \mathbf{G}^T \langle \mathbf{B} \mathbf{U}_{tj} \rangle \mathbf{G} dA \\
 &+ E_j \int_{A_j} \mathbf{G}^T \left\langle \mathbf{B} \frac{d\mathbf{U}_{tj}}{d\zeta_i} \right\rangle \mathbf{G} dA \\
 &- \frac{d\beta_j}{d\zeta_i} \int_{A_j} \mathbf{G}^T \langle \mathbf{D} \Delta \mathbf{T} \rangle \mathbf{G} dA
 \end{aligned} \tag{12}$$

where \mathbf{B} is a strain-displacement matrix.

It has been shown in Yang and Li (2013) that the direct method to obtain the derivative of \mathbf{K}_G through (12) could consume lots of computational resources for large-scale problems, basically due to the massive calculation of $d\mathbf{U}_{tj}/d\zeta_i$. The thermal displacement \mathbf{U}_t could be zero at certain iteration during the optimization, when (12) can be stated as

$$\frac{d\mathbf{K}_{Gj}}{d\zeta_i} = - \frac{d\beta_j}{d\zeta_i} \int_{A_j} \mathbf{G}^T \langle \mathbf{D} \Delta \mathbf{T} \rangle \mathbf{G} dA \tag{13}$$

Note that $\partial \beta_j / \partial \zeta_i = 0$ when $j \neq i$.

To keep the computational cost at an economical level adjoint method is employed for sensitivity analysis as described in Section 4.2.

It should be noticed that (9) and (11) are on sensitivity of simple frequency. The case of multiple frequency should be dealt individually (Seyranian et al. 1994; Rodrigues et al. 1995; Yang et al. 1999; Du and Olhoff 2007), which is briefly discussed for the problems investigated in present paper.

4.1 Mode tracking

Sensitivity analysis could be erroneous if optimization is carried out regardless of mode switching that may occur between close eigenvalues. MAC (Modal Assurance

Criteria; Ewins 1984) is adopted in this work to ensure the optimization carried out smoothly

$$MAC = \frac{\{\Phi_{\text{ref}}^T \cdot \Phi_{\text{cur}}\}^2}{\{\Phi_{\text{ref}}^T \cdot \Phi_{\text{ref}}\} \{\Phi_{\text{cur}}^T \cdot \Phi_{\text{cur}}\}} \quad (14)$$

where Φ_{ref} is reference mode shape of interest and Φ_{cur} is mode shape of currently modified structure. MAC varies between 0 and 1, and Φ_{cur} with the highest value is identified as the targeted one.

4.2 Sensitivity of natural circle frequency

The sensitivity of (simple) natural circle frequency $d\omega^2/d\zeta_i$ is first discussed by introducing the differentiation of (5) to (9) through an adjoint vector Λ_0 , that is,

$$\frac{d\omega^2}{d\zeta_i} = \Phi^T \left(\frac{d\mathbf{K}}{d\zeta_i} + \frac{d\mathbf{K}_G}{d\zeta_i} - \omega^2 \frac{d\mathbf{M}}{d\zeta_i} \right) \Phi + \Lambda_0^T \left(\mathbf{K} \frac{d\mathbf{U}_t}{d\zeta_i} + \frac{d\mathbf{K}}{d\zeta_i} \mathbf{U}_t - \frac{d\mathbf{F}_t}{d\zeta_i} \right) \quad (15)$$

It can be found that \mathbf{K}_G is function of \mathbf{U}_t , E , β , ζ ; thus (12) can be restated as,

$$\frac{d\mathbf{K}_G}{d\zeta_i} = \left(\frac{\partial \mathbf{K}_G}{\partial \mathbf{U}_t} \right)^T \frac{\partial \mathbf{U}_t}{\partial \zeta_i} + \frac{\partial \mathbf{K}_G}{\partial E} \frac{\partial E}{\partial \zeta_i} + \frac{\partial \mathbf{K}_G}{\partial \beta} \frac{\partial \beta}{\partial \zeta_i} \quad (16)$$

where \mathbf{E} , β are vectors of E and β respectively.

Equation (15) can be rearranged as

$$\begin{aligned} \frac{d\omega^2}{d\zeta_i} = & \Phi^T \left(\frac{d\mathbf{K}}{d\zeta_i} + \frac{\partial \mathbf{K}_G}{\partial E} \frac{\partial E}{\partial \zeta_i} + \frac{\partial \mathbf{K}_G}{\partial \beta} \frac{\partial \beta}{\partial \zeta_i} - \omega^2 \frac{d\mathbf{M}}{d\zeta_i} \right) \Phi \\ & + \Lambda_0^T \left(\frac{d\mathbf{K}}{d\zeta_i} \mathbf{U}_t - \frac{d\mathbf{F}_t}{d\zeta_i} \right) \\ & + \Phi^T \left(\frac{\partial \mathbf{K}_G}{\partial \mathbf{U}_t} \right)^T \frac{\partial \mathbf{U}_t}{\partial \zeta_i} \Phi + \Lambda_0^T \mathbf{K} \frac{d\mathbf{U}_t}{d\zeta_i} \end{aligned} \quad (17)$$

To avoid the calculation of the computationally expensive derivatives $\partial \mathbf{U}_t / \partial \zeta_i$, an adjoint problem (Yang and Li 2013) is defined as,

$$\mathbf{K} \Lambda_0 = -\Phi^T \left(\frac{\partial \mathbf{K}_G}{\partial \mathbf{U}_t} \right) \Phi \quad (18)$$

characterizing the adjoint variable Λ_0 . Satisfaction of this adjoint equation implies that the last two terms in (17) equal to zero,

$$\Phi^T \left(\frac{\partial \mathbf{K}_G}{\partial \mathbf{U}_t} \right)^T \frac{\partial \mathbf{U}_t}{\partial \zeta_i} \Phi + \Lambda_0^T \mathbf{K} \frac{d\mathbf{U}_t}{d\zeta_i} = \mathbf{0} \quad (19)$$

Substituting the result from (18) in (17), the derivative of natural circle frequency in its final form can be obtained,

$$\begin{aligned} \frac{d\omega^2}{d\zeta_i} = & \Phi_i^T \left(\frac{d\mathbf{K}_i}{d\zeta_i} + \frac{\partial \mathbf{K}_{Gi}}{\partial E_i} \frac{\partial E_i}{\partial \zeta_i} + \frac{\partial \mathbf{K}_{Gi}}{\partial \beta_i} \frac{\partial \beta_i}{\partial \zeta_i} - \omega^2 \frac{d\mathbf{M}_i}{d\zeta_i} \right) \Phi_i \\ & + \Lambda_{0i}^T \left(\frac{d\mathbf{K}_i}{d\zeta_i} \mathbf{U}_{ti} - \frac{d\mathbf{F}_{ti}}{d\zeta_i} \right) \end{aligned} \quad (20)$$

Note that $\partial E_j / \partial \zeta_i$, $\partial \beta_j / \partial \zeta_i$, $d\mathbf{K}_j / d\zeta_i$, $d\mathbf{M}_j / d\zeta_i$, $d\mathbf{F}_{tj} / d\zeta_i$ equal 0 when $j \neq i$.

As all the items in (20) are related to one element, the sensitivity of natural circle frequency can be easily calculated.

4.3 Sensitivity of dynamic compliance

Equation (7) can be written as follows by introducing an adjoint factor Λ_1 ,

$$\begin{aligned} \frac{dC}{d\zeta_i} = & \Psi^T \left(\frac{d\mathbf{K}}{d\zeta_i} + \frac{d\mathbf{K}_G}{d\zeta_i} - \omega^2 \frac{d\mathbf{M}}{d\zeta_i} - \frac{d\omega^2}{d\zeta_i} \mathbf{M} \right) \mathbf{U} \\ & + \Lambda_1^T \left(\mathbf{K} \frac{d\mathbf{U}_t}{d\zeta_i} + \frac{d\mathbf{K}}{d\zeta_i} \mathbf{U}_t - \frac{d\mathbf{F}_t}{d\zeta_i} \right) \end{aligned} \quad (21)$$

As in Section 4.2, the following equation can be obtained

$$\mathbf{K} \Lambda_1 = -\mathbf{U}^T \frac{\partial \mathbf{K}_G}{\partial \mathbf{U}_t} \Psi \quad (22)$$

through which Λ_1 can be obtained. Equation (21) can be then written as

$$\begin{aligned} \frac{dC}{d\zeta_i} = & \Psi_i^T \left(\frac{d\mathbf{K}_i}{d\zeta_i} + \frac{\partial \mathbf{K}_{Gi}}{\partial E_i} \frac{\partial E_i}{\partial \zeta_i} + \frac{\partial \mathbf{K}_{Gi}}{\partial \beta_i} \frac{\partial \beta_i}{\partial \zeta_i} \right. \\ & \left. - \omega^2 \frac{d\mathbf{M}_i}{d\zeta_i} - \frac{d\omega^2}{d\zeta_i} \mathbf{M}_i \right) \mathbf{U}_i \end{aligned} \quad (23)$$

$$+ \Lambda_{1i}^T \left(\frac{d\mathbf{K}_i}{d\zeta_i} \mathbf{U}_{ti} - \frac{d\mathbf{F}_{ti}}{d\zeta_i} \right) \quad (24)$$

With the adjoint method, only two equations, i.e. (20) and (22) need to be solved in the sensitivity analysis at each iteration, and the computational cost can be effectively controlled.

5 Numerical examples

A four-edge clamped bi-material plate with dimension 1 m \times 1 m \times 0.01 m is studied. The plate is subjected to a uniform temperature rise $\Delta T = T_1 - T_0$ with $T_0 = 0^\circ\text{C}$. The material properties are as follows:

$$\begin{aligned} E^{(0)} &= 70\text{GPa}, \quad \rho^{(0)} = 2650\text{kg/m}^3, \quad \alpha^{(0)} = 1.5 \times 10^{-5} \text{ }^\circ\text{C}^{-1} \\ E^{(1)} &= 210\text{GPa}, \quad \rho^{(1)} = 6500\text{kg/m}^3, \quad \alpha^{(1)} = 1.1 \times 10^{-5} \text{ }^\circ\text{C}^{-1} \end{aligned}$$

A mesh of 40 \times 40 with isoparametric 4-node element is used here, and there are 1600 design variables.

The volume fraction of material 1 is up to 50%. And the initial value of all the design variables is $\zeta_i = 0.5$.

A unit concentrated force is applied normally at a quarter point of the plate, so that all modes of interest can be excited.

GCMMA (Globally Convergent version of Method of Moving Asymptotes) algorithm (Svanberg 1995) is employed, and the penalty factor 3 is used in the RAMP

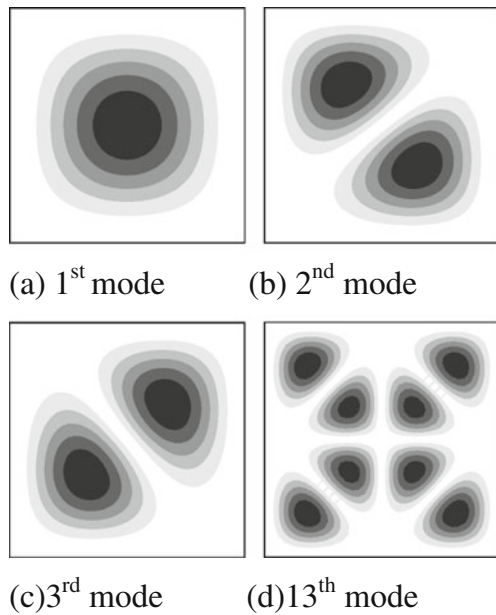


Fig. 1 Mode shapes for subcase $\Delta T = 0\text{ }^\circ\text{C}$

interpolation model. Rayleigh damp $C = 0.01(\mathbf{K} + \mathbf{K}_G)$ is considered.

5.1 Buckling and eigenvalue analysis

Critical buckling temperature $T_{cr} = 100.8\text{ }^\circ\text{C}$ with initial temperature $T_0 = 0\text{ }^\circ\text{C}$ is first evaluated through eigenvalue buckling analysis (Cook et al. 1989), to serve as upper limit of the thermal environment as the optimization is carried out in pre-buckling state. Four thermal cases, i.e. $\Delta T = 0, 50, 75, 90\text{ }^\circ\text{C}$ are chosen in this work.

Natural frequency extraction is then carried out in these thermal environments. It is known that the natural frequency of the structure may not be the resonance frequency if the corresponding mode is orthogonal to the loading mode. According to the location of the concentrated load, three resonance modes of interest are chosen, i.e. 1st, 2nd and 13th of the initial structure, which can also be verified through frequency response analysis in the following subsections.

The 1st mode is fundamental, response at which is often the most important component in dynamic analysis; the 2nd is a repeated mode; the 13th is a relatively high-order mode,

Table 1 Natural frequencies in different thermal environments (Hz)

$\Delta T/\text{ }^\circ\text{C}$	1 st	2 nd	3 rd	12 th	13 th
0	184.1	374.5	374.5	1227	1233
50	132.2	319.5	319.5	1170	1177
75	95.28	287.7	287.7	1140	1147
90	61.34	266.6	266.6	1122	1129

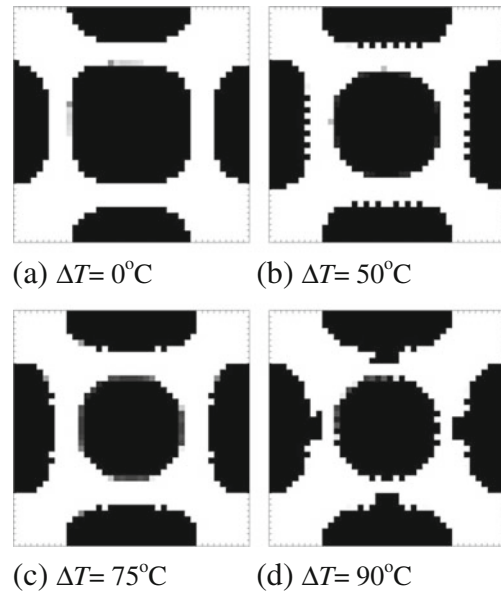


Fig. 2 Topology at 1st initial resonance frequency (white - material 0, black- material 1)

whose frequency is quite close to that of the 12th. The mode shapes are shown in Fig. 1. As the thermal environment hardly changes the mode shape of this square plate, only the mode shape with $\Delta T = 0\text{ }^\circ\text{C}$ is presented. The mode frequencies are shown in Table 1. It can be found that the natural frequencies decrease as the temperature rises, indicating a softening effect of the thermal environment.

5.2 1st initial resonance frequency

Figure 2 shows the optimal topology at the 1st initial resonance frequency. The load is applied at the up-left quarter point (1/4, 3/4) of the plate shown in the figure, despite

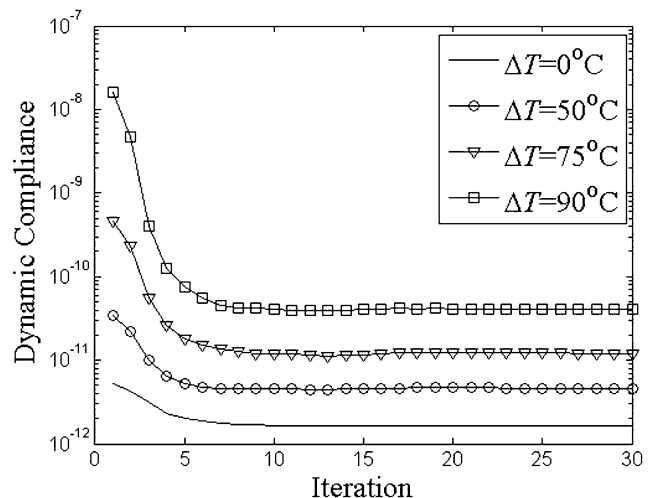


Fig. 3 Iteration history of the dynamic compliance at the 1st initial resonance frequency

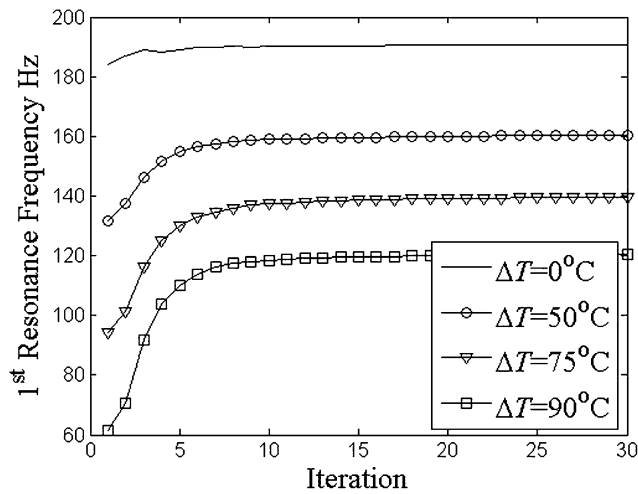


Fig. 4 Iteration history of the 1st initial resonance frequency

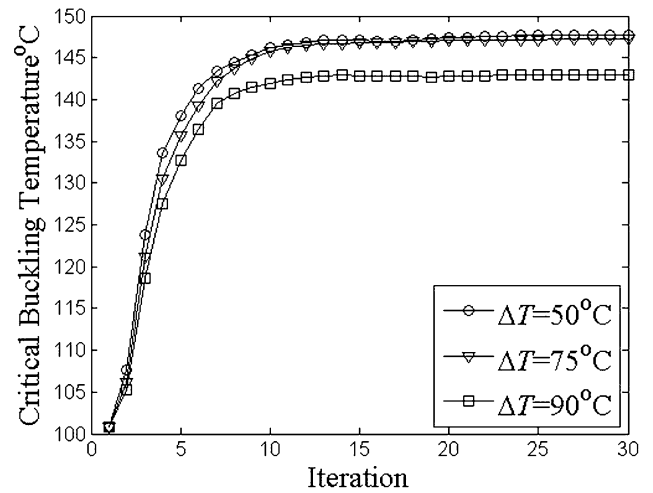


Fig. 6 Iteration history of the critical buckling temperature in the optimization at 1st initial resonance frequency

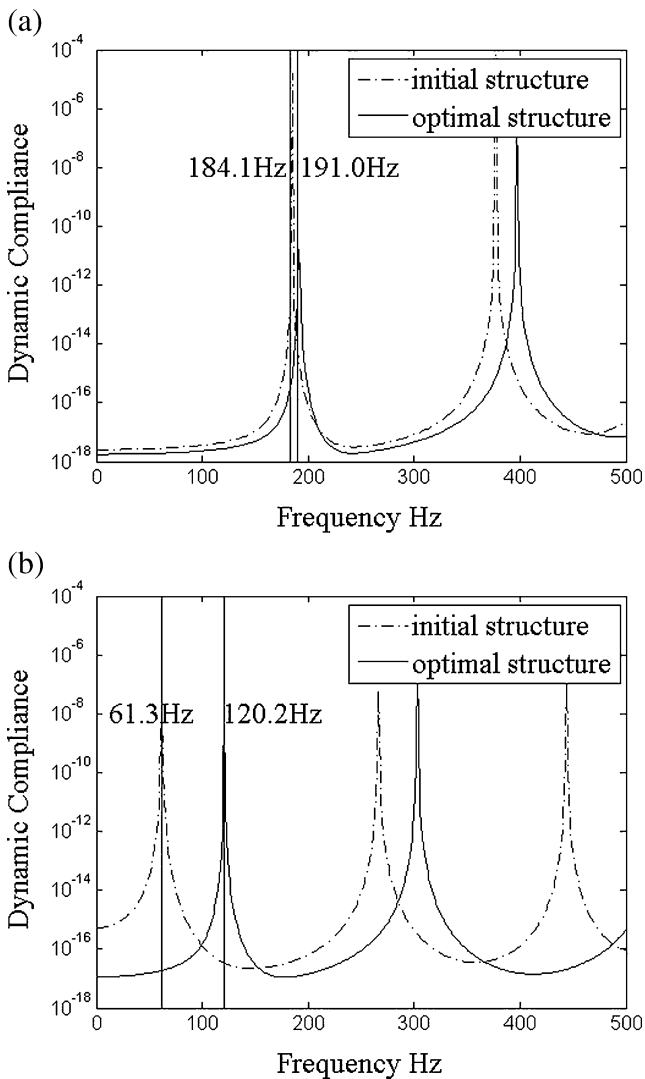


Fig. 5 Dynamic compliance of the initial structure and optimal structure in 0-500 Hz

of which the distribution of the stiffer material is basically symmetrical. As the resonance response is mainly affected by the fundamental mode, it could be concluded that the mode mainly determines the optimal topology. Some stiffer material gathers at the center, and some distributes along the edges. As the temperature rises, some stiffer material (i.e. material 1) moves outwards. Note that there is no filtering technique employed in this work, so zigzag distribution can be found in the topology. However there are few “gray” elements.

Figure 3 shows that iteration history of the dynamic compliance. It can be found that the dynamic compliance

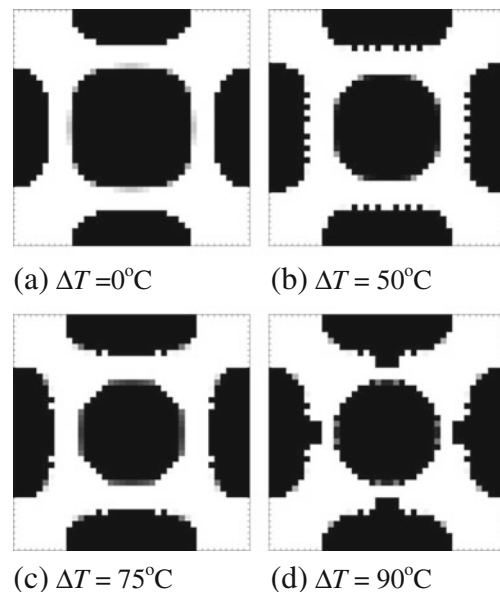


Fig. 7 Topology at 1st initial resonance frequency with the center-applied load

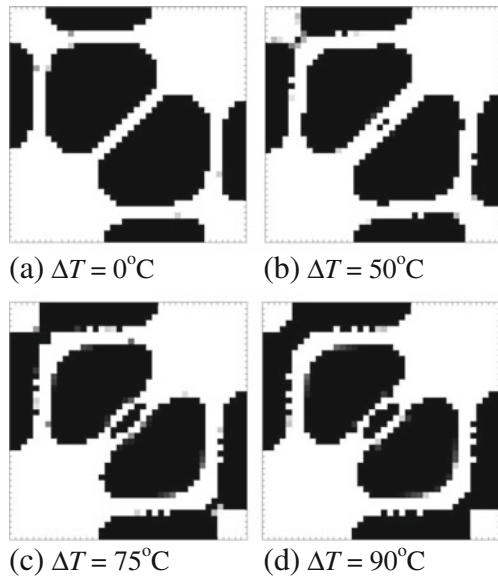


Fig. 8 Topology at 2nd initial resonance frequency (white - material 0, black- material 1)

becomes larger as the temperature rises. Since the compliance is calculated at resonance frequency, the damping mainly affects the value. In this work Rayleigh damping is used; the structure with smaller stiffness exhibits larger resonance response and dynamic compliance. Due to the softening effect of the thermal environment, the dynamic compliance of the subcase with higher temperature is larger.

Figure 4 shows the iteration history of 1st initial resonance frequencies in different environments, which increase with the iteration accumulating. As mentioned above, it could be said that the stiffer material distributes mainly according to the mode, leading to this increase.

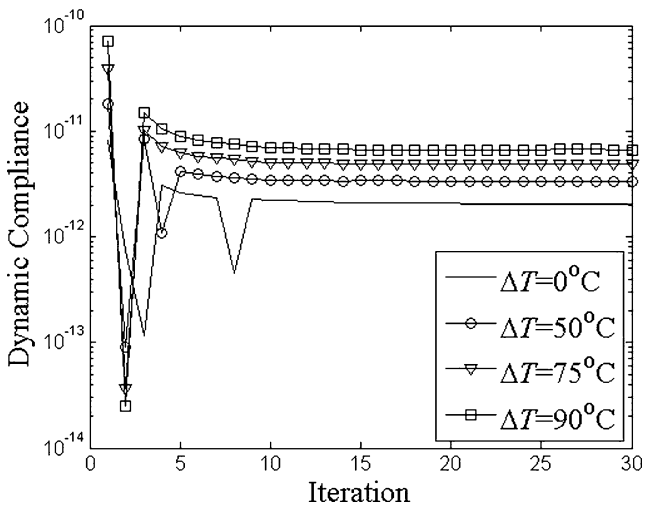


Fig. 9 Iteration history of the dynamic compliance at the 2nd initial resonance frequency

The resonance frequencies are 191.0, 160.3, 139.5 and 120.2 Hz respectively in the optimal design, suggesting that the structure becomes stiffer and the dynamic compliance gets smaller.

Figure 5 shows the dynamic compliance of the initial and optimal structure in frequency band for thermal subcases $\Delta T = 0$ and 90°C respectively. Due to the increase of the natural frequency, the peaks shift right and the dynamic compliance becomes lower in the band around the 1st initial resonance frequency, and around the others as well. It is generally meaningless to carry out comparison between values of the peaks, frequencies of which may not be the resonance frequencies, but a bit higher.

Figure 6 shows iteration history of the critical buckling temperature. Since T_{cr} increases as the optimization proceeds, the plate is always in the pre-buckling state and a linear dynamic problem can be guaranteed.

If the concentrated load is applied at the center point (1/2, 1/2) of the plate, the optimal design becomes what is shown in Fig. 7. Comparison between Figs. 2 and 7 indicates that the location of the load does not have significant influence on the optimal design at the 1st initial resonance frequency. It could be confirmed that the mode mainly affects the topology as long as it is excited.

5.3 2nd initial resonance frequency

Note that the 2nd and 3rd resonance frequencies of the initial structure are multiple, sensitivity analysis of which should be carried out with special technique due to the problem of non-differentiability. In this work, the sensitivity with respect to each single design variable is found by formulation and solution of a subeigenvalue problem (Seyranian et al. 1994) with additional consid-

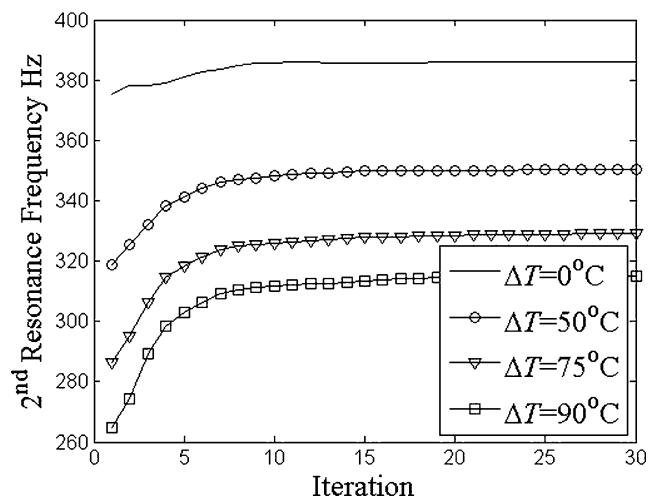


Fig. 10 Iteration history of the 2nd initial resonance frequency

eration of the thermal effect, i.e. the derivative of \mathbf{K}_G . It is noticed that the concentrated load is applied at the quarter point of the plate, indicating that the topology could not be absolutely symmetric from the 2nd iteration and the multiple frequencies will no longer be identical. At the 1st iteration there is no thermal strain as the structural material distribution is initially uniform, which means the derivative of \mathbf{K}_G could be obtained directly with (13).

Figure 8 shows the optimal topology at the 2nd initial resonance frequency. Test of orthogonality shows that the 2nd other than the 3rd initial mode ($\Phi^T \mathbf{F} = 0.223, 0.024$ respectively, for subcase $\Delta T = 0^\circ\text{C}$) exerts main influence on the resonance; thus it could be concluded from Fig. 8 that the excited 2nd mode mainly determines the topology. The increase of the temperature slightly changes the optimal design. Some stiffer material (material 1) moves towards

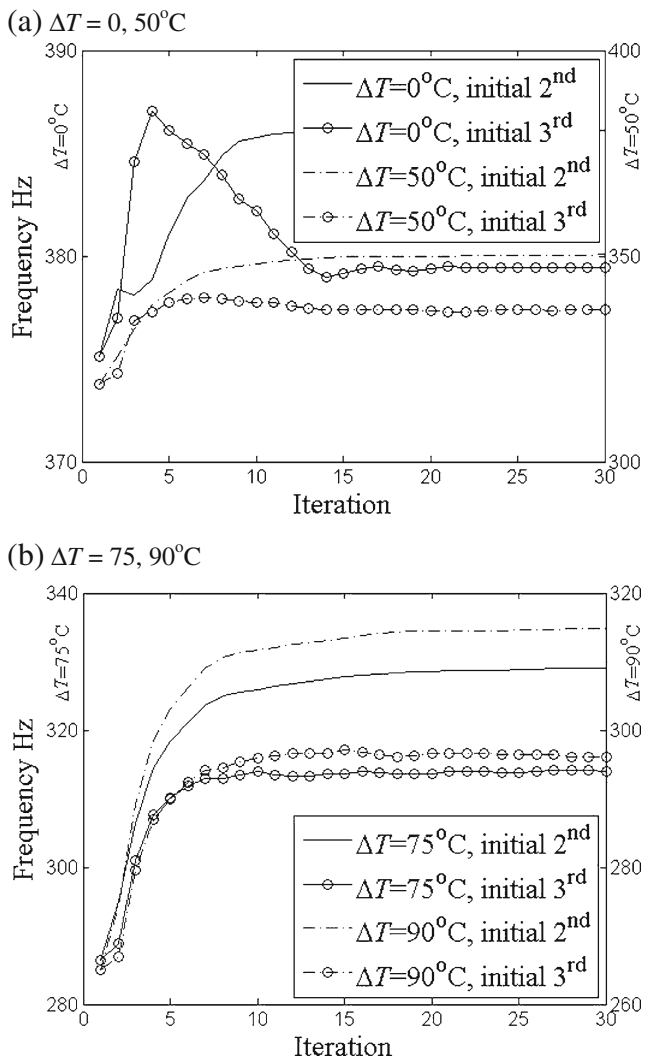


Fig. 11 Iteration history of the 2nd and 3rd initial resonance frequencies

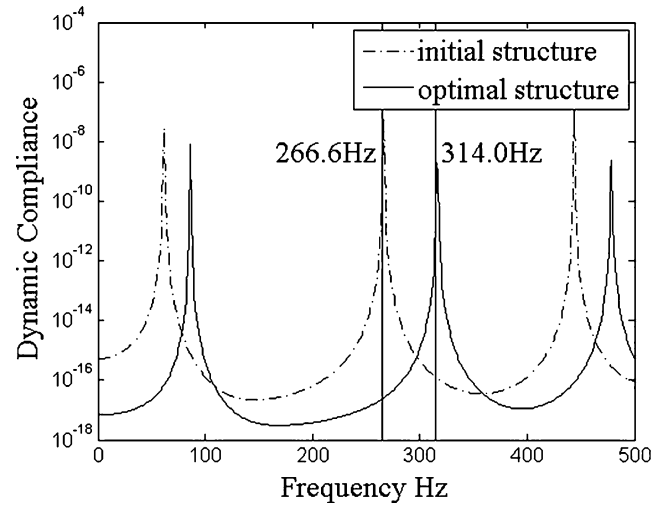


Fig. 12 Dynamic compliance of the initial structure and optimal structure in 0-500 Hz for subcase $\Delta T = 90^\circ\text{C}$

the corner and joints the margin parts together, while some appears at the center.

Figures 9 and 10 show the iteration history of the dynamic compliance and the 2nd resonance frequency respectively. The dynamic compliance of the subcase with smaller temperature change is lower, and the resonance frequency increases as the iteration accumulates; both are similar to those in precious subsection.

Figure 11 shows iteration history of the 2nd and 3rd initial resonance frequencies. It can be found that mode switching occurs, and the initial 2nd resonance frequency turns to the 3rd in the optimal design.

The two resonance frequencies may become “sufficiently close” during optimization, when problems due to non-differentiability could also occur. It could be assumed in this work that there are no “sufficiently close” eigenvalues

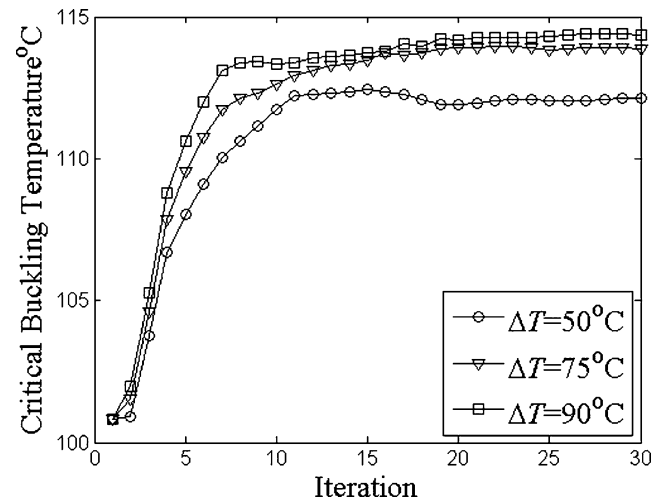


Fig. 13 Iteration history of the critical buckling temperature in the optimization at 2nd initial resonance frequency

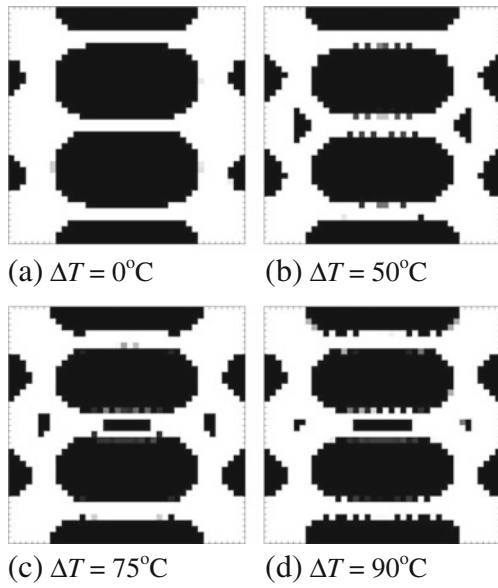


Fig. 14 Topology at 2nd initial resonance frequency with the point (1/2, 3/4)-applied load (white - material 0, black- material 1)

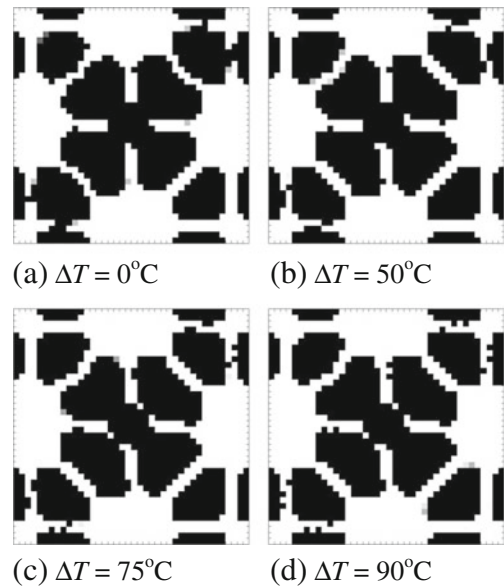


Fig. 16 Topology at 13th initial resonance frequency (white - material 0, black- material 1)

during the optimization, if the criterion on “close” is tight enough. There is no direct proof that this assumption would result in the fluctuations in Fig. 9 (for example, see the 3rd iteration of subcase $\Delta T = 0^\circ\text{C}$). In fact, it is quite normal to have fluctuations at the beginning of iteration.

Figure 12 shows the dynamic compliance of the initial and optimal structure in frequency band for thermal case $\Delta T = 90^\circ\text{C}$, demonstrating similar change of dynamic compliance to that in previous subsection. Comparison between Figs. 5(b) and 12 indicates that although the topology obtained in previous subsection could also decrease the dynamic compliance around the 2nd resonance frequency,

the topology shown in Fig. 8 yields better results.

It could be found from Fig. 12 that in the two frequencies separating from the initial multiple frequency, only the mode of the initial 2nd (or final 3rd) is excited in the optimal design, partly due to that it weighs more in the resonance response.

Figure 13 shows iteration history of the critical buckling temperature.

If the load moves from point (1/4, 3/4) to point (1/2, 3/4), the optimal topology becomes what is shown in Fig. 14. As the 2nd and the 3rd modes of the initial structure exert almost equal influence on resonance response (estimated

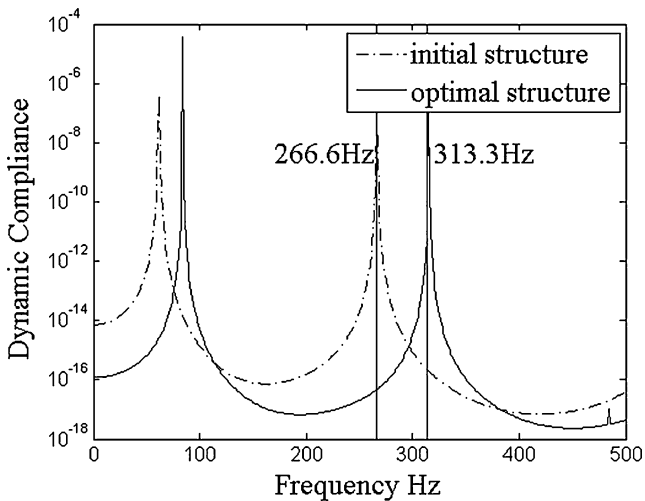


Fig. 15 Dynamic compliance of the initial structure and optimal structure in 0-500 Hz for subcase $\Delta T = 90^\circ\text{C}$

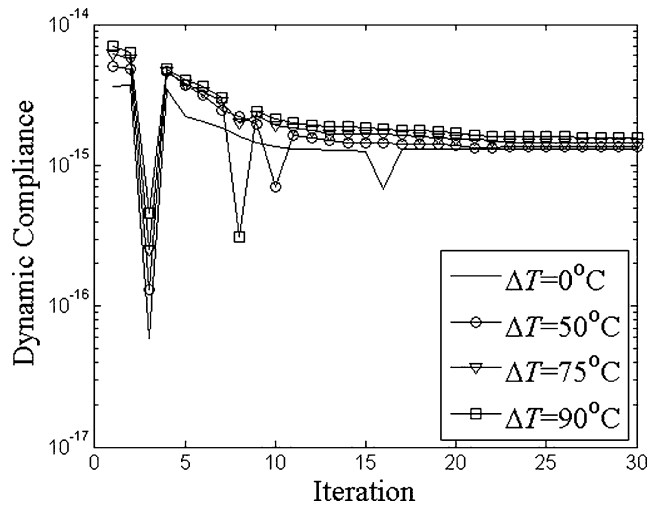


Fig. 17 Iteration history of the dynamic compliance at the 13th initial resonance frequency

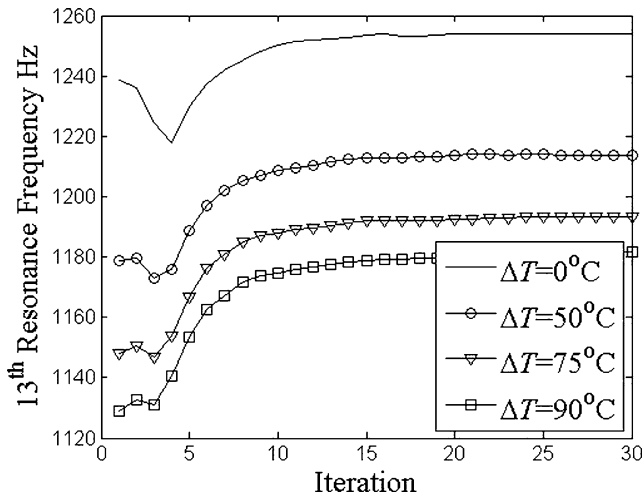
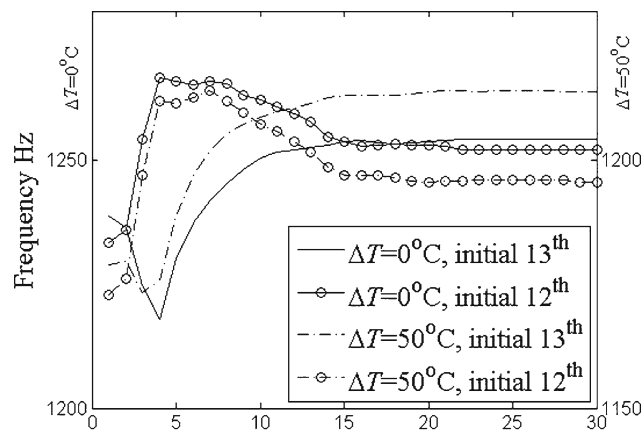


Fig. 18 Iteration history of the 13th initial resonance frequency

through test of orthogonality $\Phi^T \mathbf{F} = 0.208, 0.168$ respectively, for subcase $\Delta T = 0^\circ\text{C}$), it could be inferred that the location of the load may affect the topology through

(a) $\Delta T = 0, 50^\circ\text{C}$



(b) $\Delta T = 75, 90^\circ\text{C}$

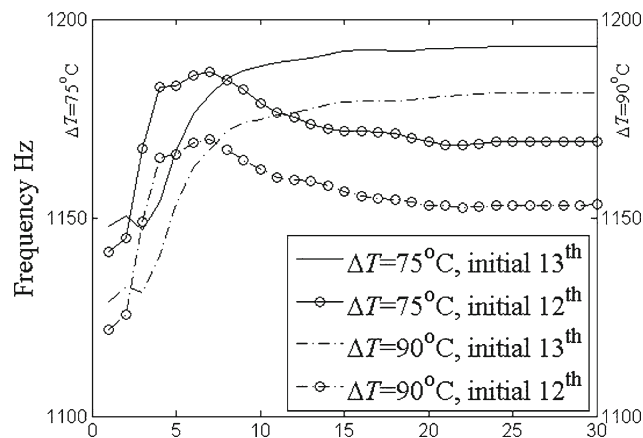


Fig. 19 Iteration history of 12th the 13th initial resonance frequencies

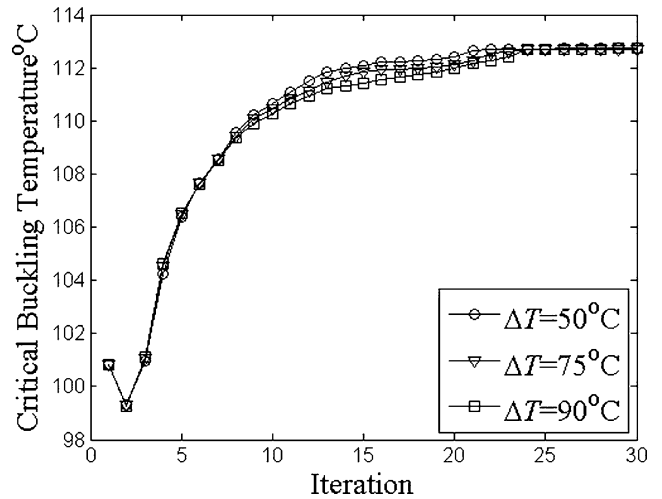


Fig. 20 Iteration history of the critical buckling temperature in the optimization at 13th initial resonance frequency

its influence on excitation of different modes. Figure 15 indicates that only the initial 2nd mode (final 3rd mode) is excited in the optimal design, like what Fig. 12 demonstrates. Although different modes may be excited at initial state of the structure, only the mode of interest is excited in the optimal design.

5.4 13th initial resonance frequency

Figure 16 shows the optimal topology at the 13th initial resonance frequency. It is quite interesting to notice that the “pattern” of topology in Fig. 16 seems to be a “combination” of that in Fig. 8, considering that the 13th initial mode shape also looks like a “combination” of the 2nd initial mode shape (see Fig. 1).

Figures 17 and 18 show the iteration history of the dynamic compliance and the 13th resonance frequency respectively; both exhibit similar change and relationship to those in the precious two subsections.

Figure 19 shows that mode switching occurs during the optimization. The 13th initial mode still keeps the same order in the optimal design, although it switches to the 12th at some iteration. Note that the situation with “sufficiently close” eigenvalues is not considered.

Figure 20 shows iteration history of the critical buckling temperature.

6 Conclusions

Topology optimization aimed at the dynamic compliance at resonance frequencies in thermal environments is carried out in this paper. The resonance response is obtained through a linear stress-stiffening dynamic finite element

formula. Adjoint method is utilized in the sensitivity analysis to improve the computational efficiency. As the resonance frequency is constantly changing during the optimization, its sensitivity is also considered.

It can be found that the dynamic compliance increases as the temperature rises, mainly due to the softening effect of the thermal stress. The optimization results in gradually growing resonance frequency leading to decreasing dynamic compliance in nearby frequency band. The optimal topology is mainly determined by the modes that are excited by applied load. For the cases investigated here, different modes may be excited initially, while only the mode of interest is excited in the optimal design. Mode switching might occur during the optimization, which is handled through mode tracking technique. The critical buckling temperature increases as the optimization proceeds, indicating the structure is always in pre-buckling state.

One of the numerical cases involves multiple natural frequencies in thermal environments, sensitivity of which is calculated in a simplified way considering change of single design variable. However, these design variables in fact change simultaneously. Besides, natural frequencies may become rather close during the optimization, which also needs additional consideration. Further research should be conducted on these issues. As the optimization carried out in this paper is aimed at the dynamic compliance, investigation on these issues is kind of beyond the scope, and admittedly difficult.

Acknowledgments The assistance on the GCMMA algorithm from Prof. Svanberg K is gratefully acknowledged, and the constructive comments from the reviewers are also highly appreciated.

References

- Belegundu AD, Salagame RR, Koopmann GH (1994) A general optimization strategy for sound power minimization. *Struct Optim* 8(2–3):113–119. doi:[10.1007/BF01743306](https://doi.org/10.1007/BF01743306)
- Bendsøe MP, Kikuchi N (1988) Generating optimal topologies in structural design using a homogenization method. *Comput Meth Appl Mech Eng* 71(2):197–224. doi:[10.1016/0045-7825\(88\)90086-2](https://doi.org/10.1016/0045-7825(88)90086-2)
- Bendsøe MP, Sigmund O (2003) *Topology optimization: theory, Methods and applications*. Springer, Berlin
- Chen S, Gu Y, Zhao G, et al. (2003) Design optimization for structural thermal buckling. *J Thermal Stresses* 26(5):479–494. doi:[10.1080/01495730390192287](https://doi.org/10.1080/01495730390192287)
- Cook RD, Malkus DS, Plesha ME (1989) *Concepts and application of finite element analysis* 3rd edn. Wiley, New York
- Diaz AR, Kikuchi N (1992) Solutions to shape and topology eigenvalue optimization using a homogenization method. *Int J Numer Meth Eng* 35(7):1487–1502
- Du J, Olhoff N (2007) Topological design of freely vibrating continuum structures for maximum values of simple and multiple eigenfrequencies and frequency gaps. *Struct Multidisc Optim* 34(2):91–110. doi:[10.1007/s00158-007-0101-y](https://doi.org/10.1007/s00158-007-0101-y)
- Ewins DJ (1984) *Modal testing: theory and practice*. Research Studies Press. Wiley, New York
- Gao T, Zhang W (2010) Topology optimization involving thermo-elastic stress loads. *Struct Multidisc Optim* 42(5):725–738. doi:[10.1007/s00158-010-0527-5](https://doi.org/10.1007/s00158-010-0527-5)
- Jog CS (2002) Topology design of structures subjected to periodic loading. *J Sound Vib* 253(3):687–709. doi:[10.1006/jsvi.2001.4075](https://doi.org/10.1006/jsvi.2001.4075)
- Ma ZD, Kikuchi N, Hagiwara I (1993) Structural topology and shape optimization for a frequency response problem. *Comput Mech* 13(3):157–174. doi:[10.1007/BF00370133](https://doi.org/10.1007/BF00370133)
- Ma ZD, Kikuchi N, Cheng HC (1995) Topological design for vibrating structures. *Comput Methods Appl Mech Eng* 121(1–4):259–280. doi:[10.1016/0045-7825\(94\)00714-X](https://doi.org/10.1016/0045-7825(94)00714-X)
- Min S, Kikuchi N, Park YC, Kim S, Chang S (1999) Optimal topology design of structures under dynamic loads. *Struct Optim* 17(2–3):208–218. doi:[10.1007/BF01195945](https://doi.org/10.1007/BF01195945)
- Pedersen NL (2001) On topology optimization of plates with prestress. *Int J Numer Meth Engng* 51:225–239. doi:[10.1002/nme.162](https://doi.org/10.1002/nme.162)
- Pedersen NL (2002) Topology optimization of laminated plates with prestress. *Comput Struct* 80:559–570. doi:[10.1016/S0045-7949\(02\)00026-3](https://doi.org/10.1016/S0045-7949(02)00026-3)
- Rodrigues HC, Guedes JM, Bendsøe MP (1995) Necessary conditions for optimal design of structures with a nonsmooth eigenvalue based criterion. *Struct Optim* 9(1):52–56. doi:[10.1007/BF01742645](https://doi.org/10.1007/BF01742645)
- Seyranian AP, Lund E, Olhoff N (1994) Multiple eigenvalues in structural optimization problems. *Struct Optim* 8(4):207–227. doi:[10.1007/BF01742705](https://doi.org/10.1007/BF01742705)
- Stolpe M, Svanberg K (2001) An alternative interpolation scheme for minimum compliance topology optimization. *Struct Multidisc Optim* 22(2):116–124. doi:[10.1007/s001580100129](https://doi.org/10.1007/s001580100129)
- Svanberg K (1995) A globally convergent version of MMA without linesearch In: *Proceedings first world congress of structural and multidisciplinary optimization*. Pergamon, Oxford, pp 9–16
- Yang XW, Li YM (2013) Topology optimization to minimize the dynamic compliance of a bi-material plate in a thermal environment. *Struct Multidisc Optim* 47(3):399–408. doi:[10.1007/s00158-012-0831-3](https://doi.org/10.1007/s00158-012-0831-3)
- Yang XY, Xie YM, Steven GP, Querin OM (1999) Topology optimization for frequencies using an evolutionary method. *J Struct Eng* 1125(12):1432–1438. doi:[10.1061/\(ASCE\)0733-9445\(1999\)125:12\(1432\)](https://doi.org/10.1061/(ASCE)0733-9445(1999)125:12(1432))